Mechanics of Materials 159 (2021) 103877

Contents lists available at ScienceDirect

Mechanics of Materials

journal homepage: www.elsevier.com/locate/mechmat

The relation between adhesion properties and network properties of hydrogels: A study based on an indentation adhesion method

Yang Lai [a], Yuhang Hu [a,b,*]

[a] George W. Woodruff School of Mechanical Engineering, Georgia Institute of Technology, 801 Ferst Drive, Atlanta, GA, 30332, USA
[b] School of Chemical and Biomolecular Engineering, Georgia Institute of Technology, 311 Ferst Drive, Atlanta, GA, 30332, USA

ARTICLE INFO

Keywords:
Hydrogel
Adhesion
Polymer network property
Indentation
AFM
Microindenter

ABSTRACT

Hydrogel adhesion plays a significant role in many applications. A systematic study of the surface interaction between hydrogels and other surfaces is of critical importance. In this study, we carry out indentation adhesion tests on polyacrylamide hydrogels of a wide range of compositions, across a wide range of contact sizes, and over a wide range of contact times. Based on a new contact model that we recently developed for hydrogels that can describe the length-dependent adhesion, we extract the adhesion properties including adhesion energy, cohesive strength and separation distance from the indentation measurements. It is found that hydrogel adhesion exhibits significant hysteresis. The possible mechanism that contributes to the time-dependent adhesion of hydrogels is discussed. It is also found that it is the cohesive strength that has a more direct correlation with the network features, rather than the conventionally discussed adhesion energy. Specifically, the cohesive strength is linearly proportional to the surface chain density for all the hydrogel compositions tested in this study. Moreover, by comparing the estimated network chain length with the separation distance obtained from the indentation measurements, it is concluded that dangling chains on the hydrogel surface are significantly longer than the length of the chains in the network and the longer chains play a more significant role in contributing to the adhesion of hydrogels.

1. Introduction

Hydrogels are crosslinked polymer networks imbibed with a large number of water molecules. Various hydrogels exist in nature as soft hydrated bio-tissues. Hydrogels are also widely used in many engineering fields, including drug delivery, microfluidics, sensors and actuators, cell culture scaffold, artificial tissues and organs, coatings on biomedical devices, and many others. In many cases, hydrogels are in contact with or bonded to other materials. In some cases, tthe surface properties of hydrogels also play important roles in carrying out other functions besides bonding. Hydrated bio-tissues such as cornea, cartilage and mucus normally have low friction to avoid excessive wear of the tissue. Synthetic hydrogels coated on biomedical devices are designed to provide low adhesion and friction to the surrounding environment. Considering the wide range of performance and applications of hydrogels, a systematic understanding of the surface interactions between hydrogels and other surfaces is of critical importance.

When a hydrogel is in contact with another surface underwater, the polymer chains on the hydrogel surface will form adhesion with the opposing surface of the material in contact. Tuning the chemistry of the polymer chains has been explored as an effective approach in altering the adhesion properties of hydrogels in the previous studies (Han et al., 2002). However, whether or how the structural properties of the polymer chains, e.g., polymer density or polymer chain length, influence hydrogels' adhesion properties have rarely been studied. Systematic experimental studies of the adhesion of hydrogels with different compositions are still in need for generating a more comprehensive understanding of the mechanism.

Among the existing experimental techniques, indentation is a good method for studying hydrogel adhesion due to the convenience in sample preparation and the flexibility of conducting tests at different length scales. Additionally, indentation is one of the very few methods that can measure the adhesion properties of weak interactions with good precisions. Previously, there have been some studies of hydrogel adhesion using the indentation method (Li et al., 2020; Shoaib and Espinosa-Marzal, 2018). However, because of the hydrated nature and the complex bulk and surface behaviors of hydrogels, many challenges

* Corresponding author. George W. Woodruff School of Mechanical Engineering, Georgia Institute of Technology, 801 Ferst Drive, Atlanta, GA, 30332, USA.
E-mail address: yuhang.hu@me.gatech.edu (Y. Hu).

https://doi.org/10.1016/j.mechmat.2021.103877
Received 30 November 2020; Received in revised form 1 March 2021; Accepted 9 April 2021
Available online 20 April 2021

still exist in modeling the indentation adhesion of hydrogels. Interpreting the interfacial properties from the indentation tests often involves analyzing the unloading force curves. As the unloading force is influenced by both the surface and bulk properties, a contact mechanics model is needed. For soft materials like hydrogels, the JKR model (Johnson et al., 1971) was commonly adopted to obtain the adhesion energy from the pull-off force measured through indentation. However, it was found in our previous work that the hydrogel exhibits significant adhesion hysteresis, and the pull-off force is length-dependent (Lai et al., 2019). The simple JKR model, or the more general cohesive-zone based Maugis-Dugdale model (Maugis, 1992), cannot correctly describe these characteristics of hydrogels, and thus cannot be used to obtain intrinsic interfacial properties of hydrogels. To describe these behaviors, we developed a modified Maugis-Dugdale model that can describe the length-dependent pull-off force: the pull-off force increases with the contact radius initially, but reaches a constant after the contact radius reaches a certain value. Using the modified model, the cohesive strength, separation distance, and adhesion energy can be extracted.

In this work, we use the modified Maugis-Dugdale model and the indentation adhesion tests developed in our previous work to further study the relationship between the surface properties of polyacrylamide hydrogels and their compositions. The polyacrylamide hydrogel is chosen as the model material here because of its wide application and simple chemical structures (Li et al., 2012). The indentation adhesion tests are carried out over a wide range of contact radii for accurate interpretation of interfacial properties. The tests are also carried out at a series of holding times to study the time dependence of the adhesion parameters. The possible mechanisms that relate the structure parameters to the adhesion parameters are discussed.

2. Experiment

2.1. Preparation of the hydrogel samples

A series of polyacrylamide hydrogels were prepared. The compositions are put into two groups, as shown in Table 1. In the first group, the initial mass concentrations of the monomer are fixed, while the initial mass concentrations of the crosslinker are different. In the second group, the initial mass concentrations of the monomer are different, but the ratio of the mass concentrations between the monomer and the crosslinker is fixed.

To make the hydrogel samples, the acrylamide solution of 40% mass concentration and N, N′- methylenebis(acrylamide) solution of 2% mass concentration were first prepared. For each hydrogel composition, the two stock solutions were mixed with DI water to attain the initial mass concentration, as listed in Table 1. The mixed solution was then added with ammonium persulfate solution (10% mass concentration) and catalyst tetramethylethylenediamine, with volume fractions of 0.5% and 0.05%, respectively. The mixture was stirred on a mixer and poured into a closed mold of 1 mm thickness. The upper and lower sides of the mold were made of clean glasses to attain the maximum similarity of the polymer chains on the hydrogel surface and in the bulk (Kii et al., 2001).

Table 1
Compositions of the polyacrylamide hydrogel samples.

No.	Initial Mass Concentration of Acrylamide	Initial Mass Concentration of N, N′- methylenebis(acrylamide)	Group
1	10%	0.1%	Group 1
2	10%	0.2%	Group 1
3	10%	0.3%	Group 1
4	10%	0.4%	Group 1
5	10%	0.5%	Group 1 Group 2
6	7.5%	0.375%	Group 2
7	5%	0.25%	Group 2

The solution was cured in the mold for an hour, and the formed hydrogel was taken out of the mold and put into DI water for a week to ensure full saturation. The mass of each hydrogel sample before and after swollen was measured separately. The swelling ratio of the hydrogel was calculated as $\lambda_{SR} = [1 + (m_{\text{swollen-gel}}/m_{\text{polymer}} - 1)\cdot(\rho_{\text{polymer}}/\rho_{\text{water}})]^{1/3}$, where ρ_{polymer}=1.443 g/cm^3 and ρ_{water}=1.0 g/cm^3. The value m_{polymer} was estimated by the mass value of the hydrogel immediately after being prepared ($m_{\text{prepared-gel}}$) and the mass concentration of the monomer (c_{m}) and crosslinker (c_{c}): $m_{\text{polymer}} = m_{\text{prepared-gel}}(c_{\text{m}} + c_{\text{c}})$. The mass concentrations c_{m} and c_{c} take the values from Table 1. They are defined as the mass concentration of the monomer or crosslinker in the mixture solution when the hydrogel is prepared.

2.2. Indentation adhesion experiment on the atomic force microscope (AFM)

To carry out indentation adhesion tests over a wide range of contact radii while maintaining the small deformation assumption to be valid, the tests were conducted on both an AFM and a microindenter, with indenters of the same material but different sphere radii (polystyrene beads, Polyscience, Inc). For tests on the AFM (Asylum MFP3D-Bio AFM), a polystyrene sphere of radius 12.5 μm was glued to the end of an AFM cantilever using a micromanipulator. The spring constant of the cantilever was calibrated by the thermal method. A fully swollen hydrogel sample was glued to a coverslip, which was then glued to the center of a petri dish. Before the experiment, both the hydrogel sample and the AFM probe were submerged in DI water for more than 6 h for the whole system to reach thermal equilibrium. The sample and the AFM probe were kept immersed in DI water throughout the test.

As is illustrated in Fig. 1(a), in the indentation adhesion test, the indenter was first driven to approach the hydrogel surface at a speed of 2 μm/s. After the surface was detected, the indenter was driven to press into the sample at a speed of 50 μm/s until a preset indentation depth was reached. Then the indentation depth was fixed for a preset amount of holding time using the closed-loop feedback built in the AFM controlling software. After the holding, the indenter was retracted at the speed of 25 μm/s. Both the indentation depth and the contact force throughout the test were recorded. One set of the representative results on the force-time curve and the force-displacement curve is illustrated in Fig. 1(c) and (e). The indentation depth used in the AFM tests spanned from 0.25 μm to 2.0 μm, and the holding time was from 1 s to 180 s. For each combination, three points on the same hydrogel surface were tested. The data acquisition rate was above 500 Hz.

2.3. Indentation adhesion experiment on the microindenter

Indentation adhesion tests with the indenter of a larger radius were conducted on a microindenter (Femto-tools, FT-MTA03 Micromechanical Testing and Assembly System). A polystyrene sphere with a radius of 200 μm was glued to the end of the force probe with a force range of 2 mN using epoxy glue. The hydrogel sample was prepared following the same method as that for the AFM test. Throughout the test, both the hydrogel and the indenter sphere were entirely submerged in water. The effect of capillary force acting on the shaft of the force probe can be calibrated and eliminated from the measurements. The details of the method were introduced in our previous paper (Lai et al., 2019).

The loading process is illustrated in Fig. 1(b) as the displacement-time curve. During the test, the indenter was driven to approach the hydrogel surface at a speed of 25 μm/s, then held at a constant indentation depth for a preset amount of holding time, and then retracted at 25 μm/s. The contact force was measured throughout the test as functions of displacement and time, at a data acquisition frequency of 3000 Hz. One set of representative results from the microindenter is illustrated in Fig. 1(d) and (f). On the microindenter, the indentation depth was chosen from 2 μm to 30 μm, and the holding time was from 1 s to

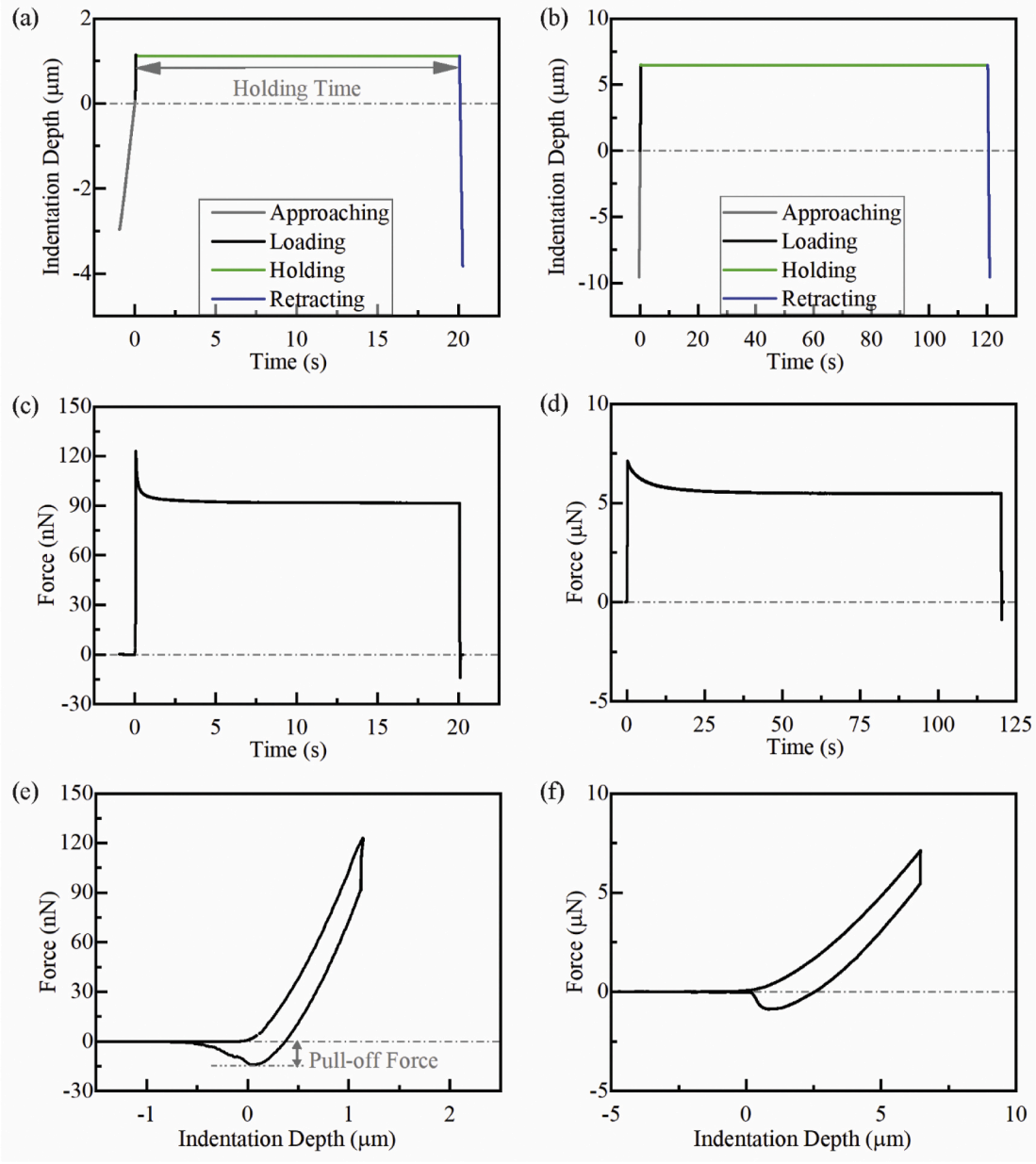

Fig. 1. The indentation depth-time relation in (a) an AFM test and (b) a microindenter test. The contact force-time relation from (c) an AFM test and (d) a microindenter test. The force-indentation depth relation from (e) an AFM test and (f) a microindenter test.

180 s. Three points on the hydrogel surface were tested for each combination of holding time and indentation depth.

3. Results and discussions

Typical force curves from the indentation adhesion tests are shown in Fig. 1. Specifically, Fig. 1(c) and (e) are the results from the AFM tests, and Fig. 1(d) and (f) are from the microindenter tests, respectively. All plots in Fig. 1 are from the hydrogel samples that have the No.1 composition as in Table 1. Fig. 1(c) and (d) show that immediately after loading, the contact force relaxes while the indentation depth is held constant. Comparing the force curves from the AFM tests (Fig. 1(c)) and those from the microindenter tests (Fig. 1(d)), the time required for the contact force to reach a constant is much longer with a larger indenter radius, i.e., a larger contact radius. The length dependence of the relaxation time indicates that the poroelasticity is dominating the time-dependent bulk behavior of the hydrogels, which is expected for polyacrylamide hydrogels. For detailed discussions of the poroelastic behaviors of hydrogels, one can refer to the previous work (He and Hu, 2020; Hu et al, 2010, 2012; Hu and Suo, 2012; Kalcioglu et al., 2012; Lai and Hu, 2017, 2018).

Fig. 1(e) and (f) also show that there exists significant hysteresis between the loading and unloading force curves, a phenomenon often called adhesion hysteresis. For the hydrogel and indenter materials used in this study, we do not observe jump-in contact during loading, indicating that the adhesion between the indenter and the gel is negligible when they initially come into contact. During unloading, the contact force first decreases to zero, and then a pulling force appears as the indenter is further retracted. The maximum pulling force is referred to as the pull-off force. In Fig. 2, the pull-off force for hydrogel sample No.1 is plotted as a function of the holding time at different indentation depths, which shows that the pull-off forces increase over the holding time for any given indentation depth, indicating that the hydrogel adhesion increases with contact time. The same trend was also observed on all the

other hydrogel samples in the current study (see Fig. S1 in the supplementary information for the results on other samples). Here, we want to emphasize that this timescale of adhesion hysteresis is independent of the bulk poroelastic behavior of the material for the following reasons. First, the pull-off force keeps increasing over the whole holding time that is much longer than the poroelastic relaxation timescale. In this study, for all the hydrogel compositions, the values of diffusivity are on the order of 1E-10 m^2/s, and the characteristic time for poroelastic relaxation is on the order of 0.1 s for the contact size carried out on AFM, and 10 s for the contact size carried out on the microindenter. Both time scales are much shorter than the hysteresis time scale observed in the experiment. Second, the slope of the pull-off force versus holding time does not change throughout the whole holding period during and after poroelastic relaxation.

Besides time-dependent adhesion, the hydrogels also exhibit length-dependent adhesion. Fig. 3 plots the pull-off force as a function of the contact radius on hydrogel sample No.1. Here the contact radius is estimated from the Hertzian contact model $c_0 = \sqrt{R\delta}$, where R is the indenter radius and δ is the indentation depth. Different colors in Fig. 3 represent the results obtained after different contact time. The results from both the AFM tests and the microindenter tests are plotted. The hollow marks in the smaller contact radius region are from the AFM tests, in which the pull-off force increases with the contact radius significantly. The solid marks in the larger contact radius region are from the microindenter tests, and the pull-off force first slightly increases with the contact radius and then reaches a plateau. The same pull-off force versus contact radius relation was also observed on all the other hydrogel samples in this study (see Fig. S2 in supplementary information).

This relation could not be explained using the widely used JKR model (Johnson et al., 1971) or the Maugis-Dugdale model (Maugis, 1992), which predicts constant pull-off force for a particular indenter radius, regardless of the contact radius. This length-dependent adhesion could not be due to the elastocapillary effect (Chakrabarti and Chaudhury, 2013) or the osmocapillary effect (Liu and Suo, 2016) as in previous studies either, because both the hydrogel and the indenter were submerged in water. The surface tension of a hydrogel in the underwater condition is negligible, and there is no phase separation on the hydrogel surface causing the osmocapillary effect. In our previous study (Lai et al., 2019), a modified Maugis-Dugdale model was developed that is able to describe this length-dependent adhesion. We assumed that, during the holding period, the hydrogel adhesion increases by forming more adhesion sites within the contact area, and the contact profile remains the same during holding. This assumption is supported by the observation that the contact force during holding is not affected by the increased adhesion over time. Therefore, the contact radius maintains

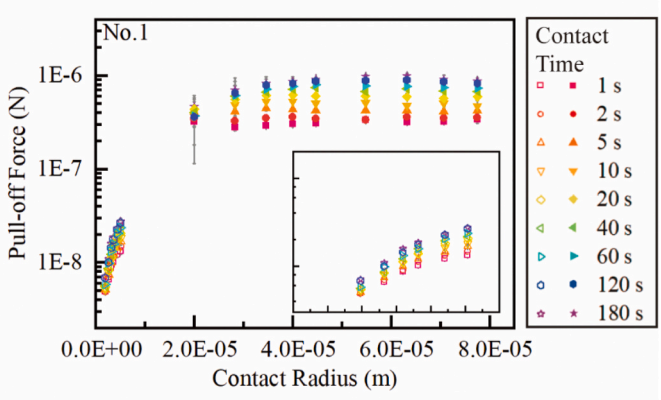

Fig. 3. The pull-off forces are plotted against the initial contact radii from the tests on the hydrogel samples of No.1 composition. Different colors represent data acquired from different holding time. The hollow marks are results from the AFM tests, and the solid marks are results from the microindenter tests. The inserted figure enlarges the results from the AFM tests. (For interpretation of the references to color in this figure legend, the reader is referred to the Web version of this article.)

the initial value c_0 as estimated by the Hertzian contact model. As for the unloading process, our previous study showed that the force curve for unloading has different characters depending on the value of the initial contact radius c_0 in comparison with a characteristic value of the contact system $c^* = (\pi\omega R^2/K)^{1/3} \cdot f(\lambda)$. Here, ω is the adhesion energy, R is the indenter radius, K is the reduced modulus of the hydrogel $K = 4E/[3(1-\nu^2)]$, with E and ν being the Young's modulus, and Poisson's ratio of the hydrogel. The term $f(\lambda)$ is a function of the nondimensional parameter $\lambda = 2\sigma_0/(\pi\omega K^2/R)^{1/3}$ that was originally introduced in the Maugis-Dugdale model. At the beginning of the unloading process, as the indenter is lifted, a cohesive zone appears at the edge of the initial contact area: the distance between the two surfaces at the outer region of contact gradually increases and attractive interaction is generated in the outer region. As the indenter is lifted further, the cohesive zone expands inwards laterally until the distance between the surfaces at the edge of the initial contact area reaches a critical value: the separation distance. At this moment, the cohesive zone is fully developed. After that, as the indenter is lifted further, the cohesive tethers break at the outer region, and the cohesive zone propagates inwards. If the original contact radius c_0 is much larger than c^* (Fig. 4(a)), after the cohesive zone is fully developed, the inner contact region where the interaction between the indenter and the gel is compressive is still relatively large. As the indenter is raised up, both compressive interaction and cohesive

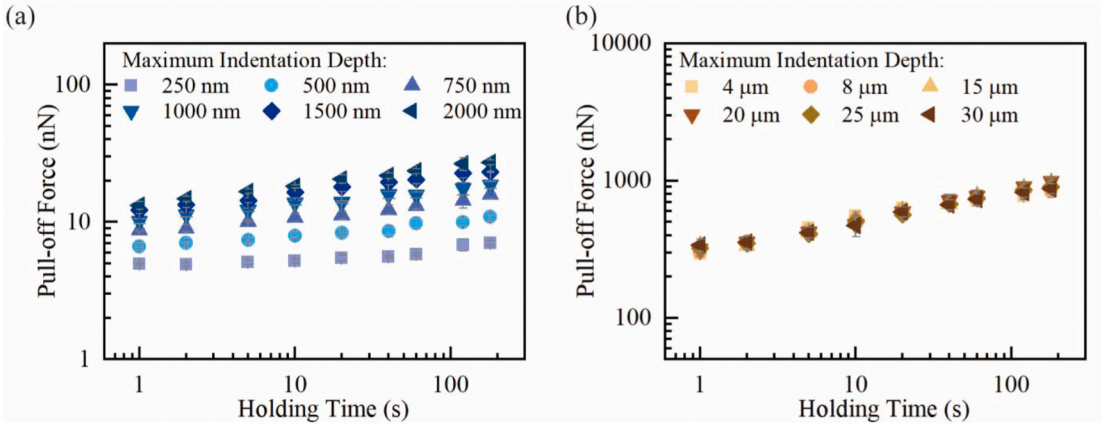

Fig. 2. The pull-off forces are plotted against the holding time for the hydrogel samples of No.1 composition at different indentation depths: (a) results from the AFM tests, (b) results from the microindenter tests.

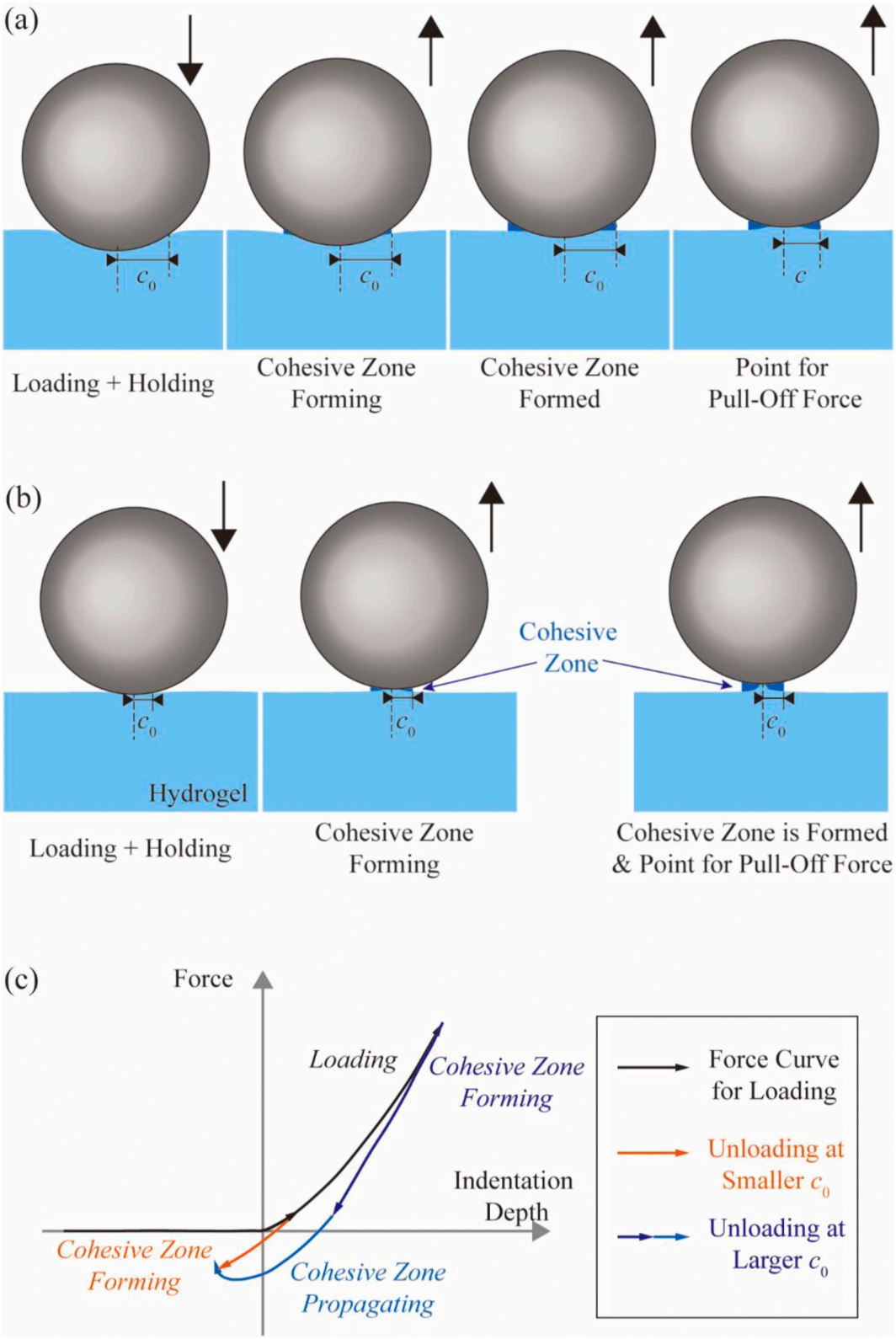

Fig. 4. (a) Illustration of the unloading process when the initial contact radius is relatively large. The pull-off force point happens after the cohesive zone is formed and is steadily propagating. (b) Illustration of the unloading process when the initial contact radius is relatively small. The pull-off force point happens immediately as the cohesive zone is formed. (c) The force-displacement relation of the loading-unloading process at different initial contact radii.

attraction decrease. In the beginning, the decrease of the compressive force is dominant, thus, the overall attractive force on the indenter increases, but later when the contact area becomes very small, the decrease of the cohesive attractions becomes dominant and the overall attractive force on the indenter decreases. Therefore, there exists a maximum value of the overall attractive force on the indenter throughout the lifting process, which is the so-called pull-off force (Fig. 4 (c)). This maximum value is independent of the size of the initial contact. In contrast, if the initial contact radius c_0 is smaller than c^* (Fig. 4 (b)), after the cohesive zone is fully developed, the inner compressive region is already very small or none, and as the indenter is lifted further, the decrease of the cohesive attraction is dominant and the overall attractive force on the indenter decreases. Therefore, the maximum pull-off force is the force on the indenter at the moment when the cohesive zone is fully formed, and this maximum value depends on the cohesive zone size when it is fully formed, and thus depends on the original contact radius c_0 (Fig. 4(c)).

Following the physical picture described above, in our previous study, the pull-off force versus initial contact radius relation was calculated. Essentially, the unloading process in our modified model differs from the original Maugis-Dugdale model in that we considered an initial stage when a cohesive zone develops from none. This means that during unloading, attractive forces are developed starting from the outer edge of the initial contact and propagating inward, while the contact size is maintained until the distance between the indenter and the material at the outer edge reaches a specific value (i.e. separation distance). In contrast, the original Maugis-Dugdale model considers the case that during unloading at any depth of indentation, there is a fully developed cohesive zone. As a result, the two contacting surfaces separate steadily, and the radius of the outer edge of the contact area keeps decreasing during unloading. In our modified model, to obtain the full force-displacement relation during unloading, we first calculated the force-displacement relation when the cohesive zone starts to develop from none. This force-displacement relation was solved by eliminating the stress concentration in the cohesive zone, while the contact size is kept fixed until the distance between the two surfaces at the outer edge reaches the value of separation distance. At this point, the cohesive zone is fully developed, so the rest of the force-displacement relation then transits to the relation described by the original Maugis-Dugdale model. According to the definition, the maximum attractive force through the entire force-displacement curve is the pull-off force. If the contact size is relatively large ($c_0>c^*$), the force-displacement curve for the cohesive zone development (dark blue curve in Fig. 4(c)) intersect with the Maugis-Dugdale curve (light blue curve in Fig. 4(c)) before the maximum attractive force in the Maugis-Dugdale curve is reached, the pull-off force takes the value in the Maugis-Dugdale model, which is independent of the initial contact size. If the contact size is relatively small ($c_0<c^*$), the force-displacement curve for the cohesive zone development (orange curve in Fig. 4(c)) intersect with the Maugis-Dugdale curve at a point that already passes the maximum attractive force point (lowest point) on the Maugis-Dugdale curve. In this case, the force value of the intersection point becomes the new pull-off force value rather than the maximum attractive force in the Maugis-Dugdale curve, and the force value at the intersection point is smaller for a smaller initial contact size. As a result, the pull-off force in relation to the initial contact size first increases and then reaches a plateau, which agrees with the experimental trend shown in Fig. 3. For the numerical result, the normalized pull-off force $\overline{F} = F/(\pi\omega R)$ is a function of two parameters: one is the normalized initial contact radius $\overline{c_0} = c_0/(\pi\omega R^2/K)^{1/3}$, and the other is the non-dimensional parameter $\lambda = 2\sigma_0/(\pi\omega K^2/R)^{1/3}$. For a fixed value of λ, $\overline{F}$ increases with $\overline{c_0}$ and then reaches a plateau. This numerical result does not have an explicit expression, but is obtained as a series of discrete values of related parameters. The details regarding the computation should refer to our previous paper (Lai et al., 2019). To extract material parameters, we first fit the experimentally measured pull-off force versus initial contact radius with the numerical results to extract adhesion energy ω and the parameter λ, and then obtain the separation distance by dividing the adhesion energy by the cohesive strength σ_0.

In the current study, by comparing the experimental results of the pull-off forces measured across a wide range of contact radii with the theoretical prediction from the model, we obtain the adhesion energy, cohesive strength, and separation distance of the hydrogels used in this study for different holding times. Fig. 5 shows one set of the experimental data and the fitting curves for the hydrogel samples that have the composition as the No.1 composition in Table 1. The red, yellow, and blue curves correspond to the results for three holding time: 2 s, 20 s, and 120 s, respectively. The experimental results from AFM and microindenter use indenters of different radii, so two fitting curves are generated based on the model, with the same set of adhesion properties. Fig. 5 shows that the model fits the experimental results very well. The results for hydrogels of other compositions show a similar time and length-dependent behavior. Therefore, the adhesion properties of other hydrogel samples at different holding times are also obtained through the same approach. The results are summarized in Fig. 6. The results for the two groups of hydrogels are plotted in two figures for clarity. The first group has the same initial monomer concentration but different crosslinker densities, and the second group has different monomer concentrations but keeps the same monomer to crosslinker ratio.

A clear observation from Fig. 6 is that all the adhesion properties including adhesion energy, cohesive strength and the separation distance increase with the holding time. The maximum holding time carried out in the experiments is 180 s. Longer than that, thermal drift may affect the accuracy of measurement. No plateau values of the adhesion properties are obtained within this observed period of holding, which indicates that the time scale for the adhesion hysteresis should be even longer than 180 s. First, since this adhesion hysteresis time scale is much longer than the poroelastic relaxation time scale as discussed earlier, the poroelasticity (i.e. the flow of solvent) is not the influencing factor for the increase of adhesion. In previous studies on hydrogel friction, another time scale was discussed related to the adsorption of one polymer chain onto a surface, which is the single chain relaxation time (Gennes, 1979; Gong and Osada, 1998; Pitenis et al., 2014). Its value is estimated through the relation $\tau_{sg} = \xi^3\eta/k_BT$, where ξ is the polymer chain size, η is the dynamic viscosity of water, k_B is the Boltzmann constant and T is the absolute temperature. For hydrogels, the typical chain size of the network is in the order of 10 nm–100 nm, so the single

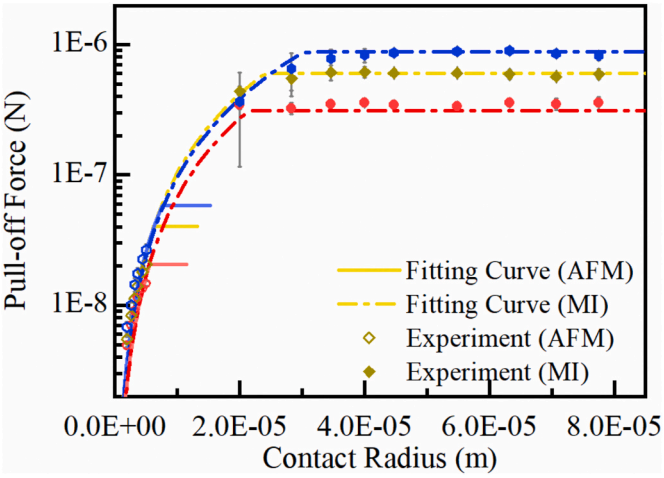

Fig. 5. The theoretical fitting curve and the experimental results of pull-off force versus contact radius for the holding time of 2 s (red), 20 s (yellow), and 120 s (blue) for the hydrogel sample of No.1 composition. (For interpretation of the references to color in this figure legend, the reader is referred to the Web version of this article.)

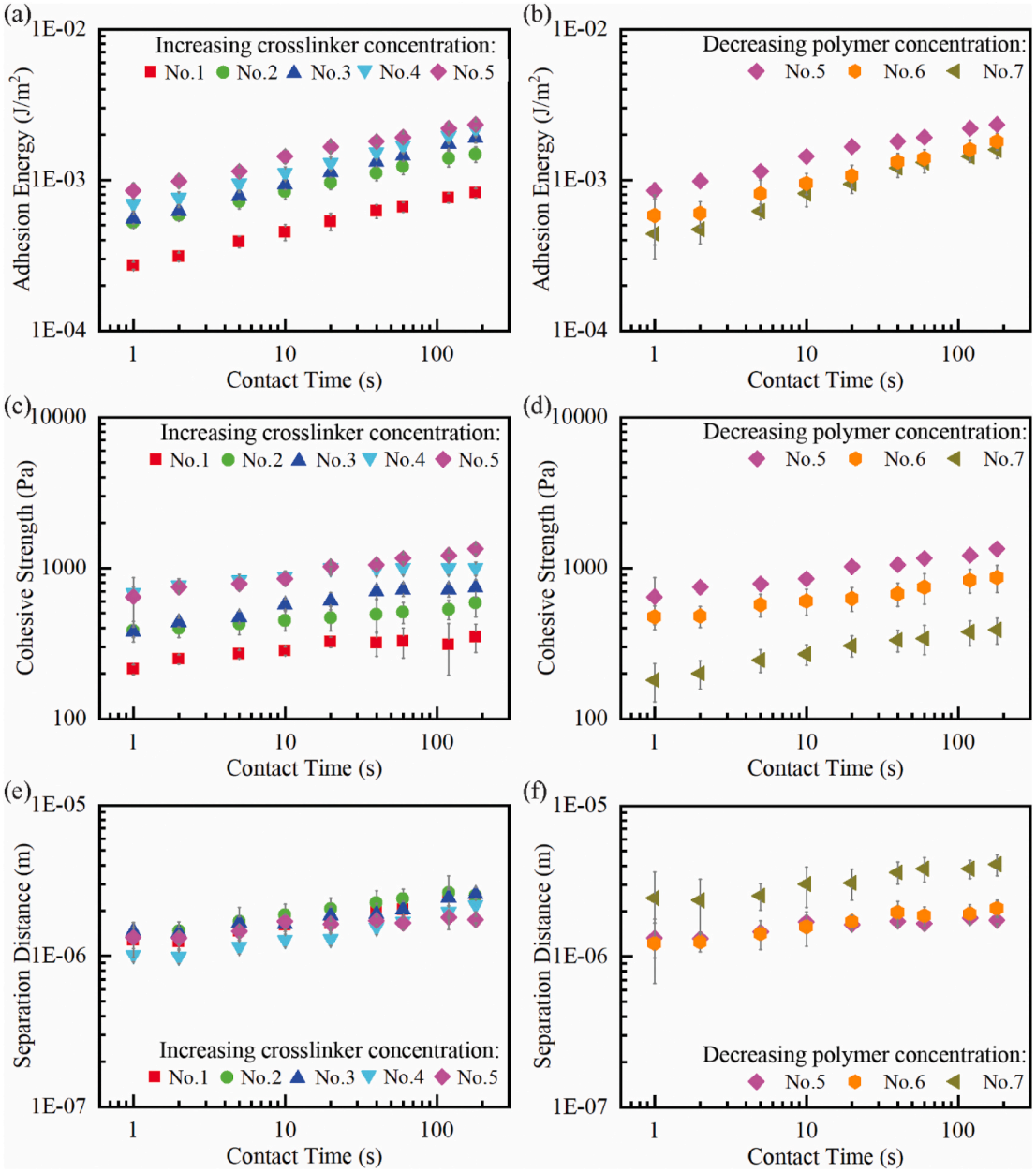

Fig. 6. Adhesion energy versus holding time for (a) the first group and (b) the second group of hydrogel samples. Cohesive strength versus holding time for (c) the first group and (d) the second group of hydrogel samples. Separation distance versus holding time for (e) the first group and (f) the second group of hydrogel samples.

chain relaxation time would be on the order of 0.0002 s–0.2 s, which is still much smaller than the time scale for the increase of adhesion observed in this study. Here, we propose a different mechanism for the hydrogel adhesion hysteresis. The illustration is shown in Fig. 7. Before contact, the surface polymer chains are in the stress-free state (Fig. 7(a)). Upon loading, the indenter is pressed onto the hydrogel surface, and the polymer chains on the surface are deformed (Fig. 7(b)). The hydrogel used in this study is polyacrylamide hydrogel. The backbone of the hydrogel's polymer chains is hydrophobic despite the overall hydrophilic nature of the polymeric network. The indenter sphere is made of polystyrene, which is also hydrophobic. It is expected that the hydrophobic parts of the polymer backbone of the hydrogel and the indenter surface generate hydrophobic interactions, which essentially involves the reorganization of the water molecules between the two hydrophobic parts to generate attractions between the two surfaces and reduce the overall system energy, (Israelachvili, 2015). According to this physical picture, along a long polymer chain, many adhesion sites can be formed between the indenter and the polymer chain, but this process takes time. This physical picture has been suggested by previous research on the adsorption of single polymer chain to a surface via molecular dynamics simulation (Yang et al., 2014), and the time scale for the increase of adhesion may be related to a stochastic effect (Lin et al., 2014; Wei, 2014) – the polymer chains tend to deform and adhere to the indenter surface, while the chain segments also have the possibility of detaching from the indenter due to thermal fluctuation. The combination of the two factors leads to an increase of adhesion over time until an equilibrium state is reached. In a short time range, very few adhesion sites (marked as the orange circles) are formed, on a few polymer chains (Fig. 7(c)). As time goes, more and more polymer chains start to develop adhesion with the indenter, and more and more adhesion sites are formed on the already adhered polymer chains with the parts that are close to the initially formed adhesion sites having a higher probability to make contact and form additional adhesion with the indenter. As more adhesion sites are formed, the force to break all the adhesion sites

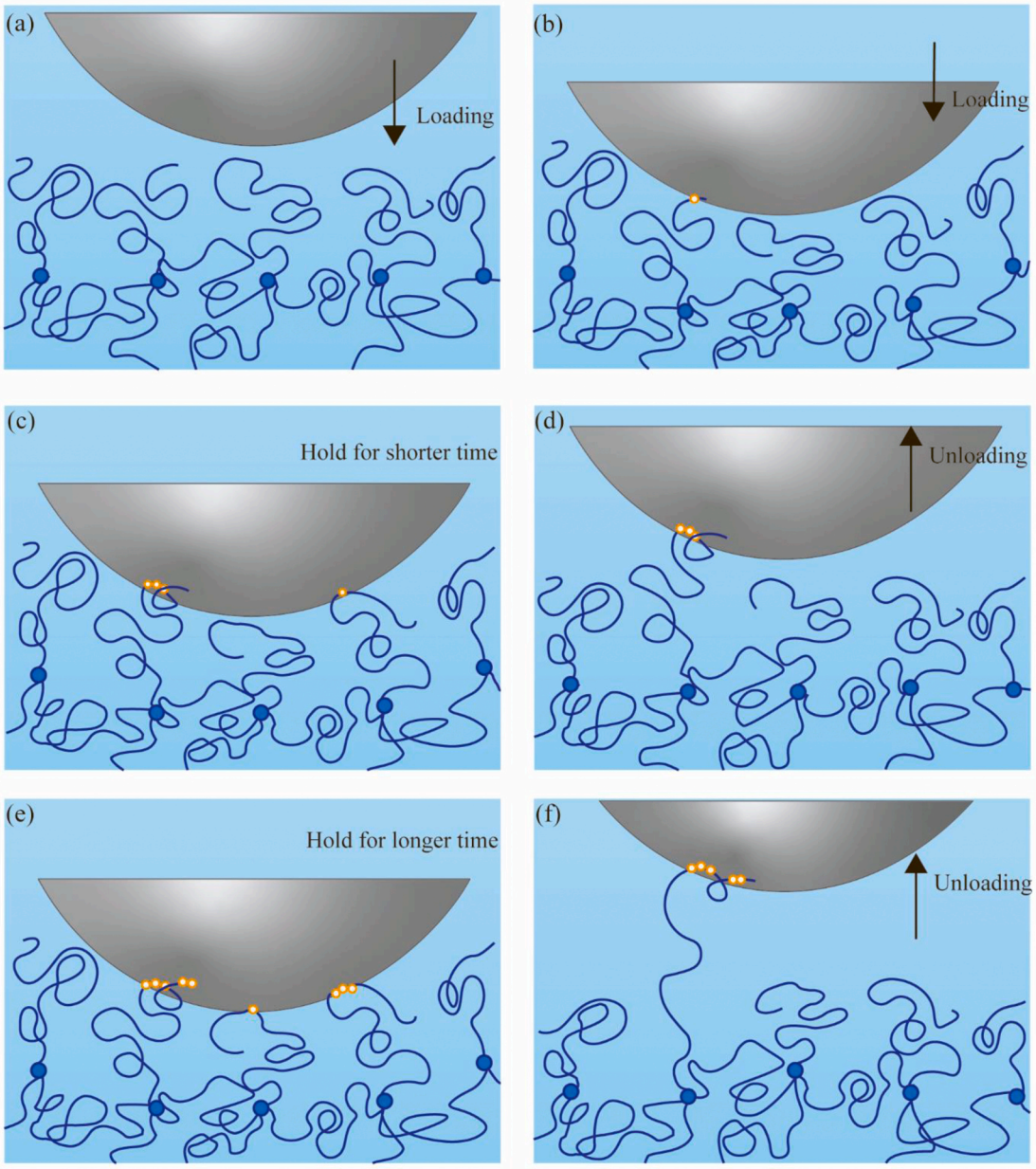

Fig. 7. Illustration of the time-dependent adhesion mechanism. The gray semi-sphere represents the indenter surface. The indenter is not drawn in the real scale to the polymer chain size, but to represent the relative distance from the gel in different stages. The dark blue lines are polymer chains, the dark blue circles are crosslinkers, the orange circles represent adhesion sites between the polymer and the indenter. (a) Before contact, the polymer chain on the hydrogel surface is in a stress-free state. (b) Upon contact, the polymer chain is deformed and a few initial adhesion sites are formed on a few polymer chains. (c) After a relatively short holding time, the polymer chains with the initial adhesive sites form more adhesion sites, some polymer chains without initial adhesion sites also start to form adhesion sites. (d) Upon unloading, the polymer chain is stretched until pulled off. (e) After a longer holding time, more adhesion sites are formed on the already adhered polymer chains, more surface polymer chains have adhesion sites with the indenter in general. (f) When unloading after a longer holding time, the polymer chain can be stretched more compared with the short holding time case before it is pulled off from the contact surface. (For interpretation of the references to color in this figure legend, the reader is referred to the Web version of this article.)

between the indenter and the hydrogel surface increases, thus increasing the cohesive strength. With more adhesion sites being formed on a single chain, the polymer chain can extend longer before it breaks all the adhesion sites from the indenter, so the separation distance will also increase over time.

We next examine the relationship between the three adhesion properties (i.e. adhesion energy, cohesive strength, separation distance) and the structural parameters of the polymer chains including the polymer mass concentration of the hydrogels at the swollen state, the average surface chain density, and the average polymer chain length. The polymer mass concentration is estimated by dividing the mass of the polymer in a sample by the total mass of the sample in its swollen state. The surface chain density of a hydrogel at equilibrium state is estimated from the bulk polymer chain density following the Flory-Rehner model (Flory, 1953; Rubinstein and Colby, 2003) by $s = N^{2/3}/{\lambda_{SR}}^2$, where N is the bulk polymer chain density that is calculated from $N = G\lambda_{SR}/k_BT$, where G is the shear modulus of the swollen gel calculated by fitting the loading force curve with the Hertzian contact model (fitting curves and results are shown in the Supplementary Information Fig. S3), λ_{SR} is the linear swelling ratio of the hydrogel, k_B is the Boltzmann constant and T

is the absolute temperature. Here it is assumed that the polymer chain density is similar to that in the bulk, which was previously proved a valid assumption for hydrogels cured against a hydrophilic cover surface (e.g. glass) (Kii et al., 2001). The third structural parameter that is considered in this study is the average polymer chain length. For the chain length without pulling force on its two ends, it is estimated using the equation $l_f = \sqrt{C_\infty \cdot 2 \cdot n} l_{cb}$, where $C_\infty = 8.5$ is the Flory's characteristic ratio of polyacrylamide chains (Bohdanecký et al., 1983), $l_{cb} = 0.154$ nm is the length of the carbon-carbon bond in the polymer chain, and n is the average number of monomers per polymer chain estimated as $n = N_A \rho_{polymer} M/N$ (Rubinstein and Colby, 2003). Here $\rho_{polymer}$ is the density of dry polymer, M is the molar mass of the monomer acrylamide, N is the bulk polymer chain density and N_A is the Avogadro constant. The estimation of n assumes that all the monomers participate in forming the polymer network (Gundogan et al., 2004). When a polymer chain is pulled using a small force, the deformation is also on the scale of l_f. The straightened chain length, on the other hand, refers to the length of a polymer chain when it is pulled using a large force so that the polymer chain is nearly fully straightened. It is estimated as $l_s = n l_{cb} \cos(\theta/2)$, where $\theta = 68°$ is the angle between neighboring carbon bonds (Rubinstein and Colby, 2003).

In most of the previous studies, it is the adhesion energy that people often extract from the adhesion measurement. Based on the new model used in the current study, besides the adhesion energy, we can further get the cohesive strength and separation distance. In fact, the experimental results show that it is the cohesive strength that has a more direct correlation with the molecular structures of the hydrogels rather than the adhesion energy. This conclusion is obtained by comparing the results in Fig. 8 and Fig. 9. Fig. 8 plots the adhesion energy of the two groups of hydrogel samples for 180 s holding time. The blue squares correspond to the results from the first group of hydrogels and the orange circles correspond to the results from the second group of hydrogels. It is shown that in both the adhesion energy versus the polymer concentration plot and the adhesion energy versus the surface chain density plot, the adhesion energy increases, but the increasing slope is different for the two groups of hydrogels. On the contrary, we observe a clear correlation between the cohesive strength and surface chain density, as shown in Fig. 9(b). For all the hydrogel samples, the cohesive strength is proportional to the surface chain density, with a constant slope and the fitting curve passing through the zero point. This observation holds not only for the contact time of 180 s, but for all the contact time (see the results of other contact time in Supplementary Information Fig. S4 and Fig. S5). The slope is bigger for a longer contact time.

We next discuss the interpretation of the separation distance. It refers to the length within which the two surfaces still have adhesive interaction. In the case of hydrogel adhesion, it is assumed that a finite separation distance exists because the surface polymer chains can extend to a longer distance from the surface to maintain the bonding with the contacting surface. Therefore, it is expected that the separation distance is related to the deformed length of a polymer chain upon surface separation. In Fig. 10(a) and (b), we plot the separation distance calculated at 180 s contact time against the average polymer chain size and the straightened chain length, respectively. The two plots show that the separation distance obtained roughly increases with the average chain size or the straightened chain length, suggesting that the separation distance is related to the polymer chain length. Similar trends are found on shorter contact time (Supplementary Information Fig. S6). However, the magnitude of the separation distance is much larger than both of the chain length parameters. One indication of the observations from Fig. 10 is that due to free-radical polymerization, the polymer chain length distribution is heterogeneous (Hamzehlou et al., 2013; Lu et al., 1993), and the longer chains play a more significant role in forming adhesion. Another indication of these observations is that since the polymer chain length is estimated based on the bulk properties of the network, it mostly reflects the length of the chain in the bulk network, but the dangling chains on the surface may be longer than the ones in the network.

4. Conclusion

Indentation adhesion measurements were carried out on polyacrylamide hydrogels of different compositions over a wide range of holding times and contact radius. Based on the modified Maugis-Dugdale model, the adhesion properties including the adhesion energy, the cohesive strength, and the separation distance were extracted from the experimental results. The adhesion parameters obtained through this approach are intrinsic to the hydrogel surface property. Significant adhesion hysteresis was observed and a possible mechanism was discussed. It was also found that the cohesive strength rather than the traditionally focused parameter of adhesion energy has closer correlations with the network structural properties of the hydrogels. Specifically, the cohesive strength value scales linearly with the surface polymer chain density with the same slope for all the gels of different compositions. It was also found that extracted separation distance is much longer than the length of the polymer chain estimated for the bulk network, suggesting that the dangling chains on the surface are longer than the network chain length.

Author statement

Yang Lai: Methodology, Analysis, Investigation, Writing of original Draft, Experiments. Yuhang Hu: Resources, Writing - Review & Editing, Supervision, Funding acquisition.

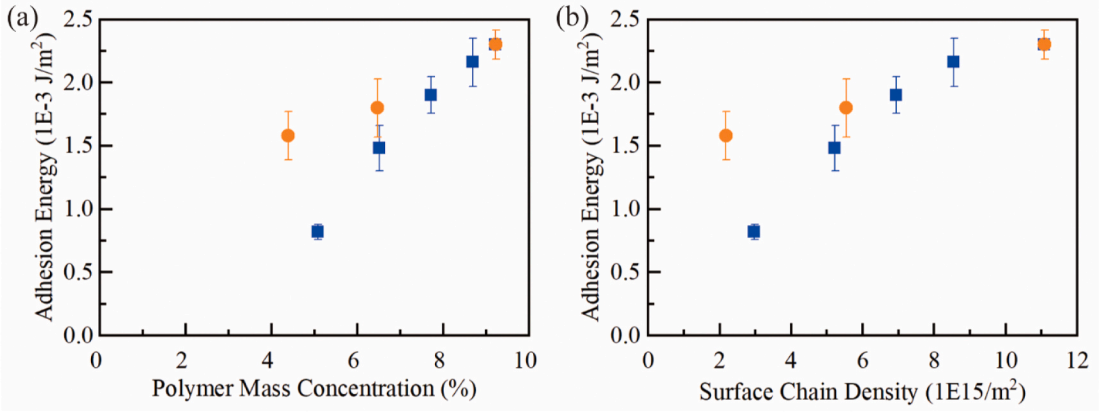

Fig. 8. (a) Adhesion energy versus polymer concentration. (b) Adhesion energy versus surface chain density. Results are from the holding time of 180 s. The data point for sample No.5 that occurs in both groups is the most right one in both plot (a) and plot (b).

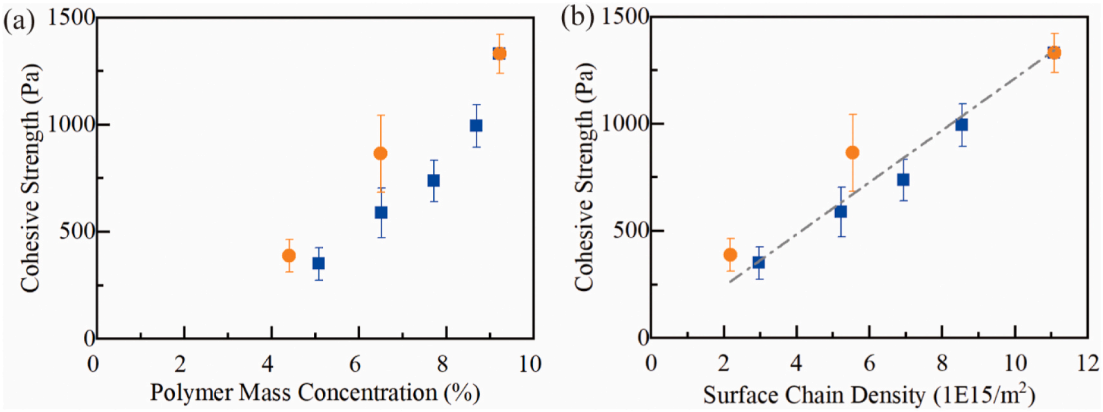

Fig. 9. (a) Cohesive strength versus polymer concentration. (b) Cohesive strength versus surface chain density. Results are from the holding time of 180 s. The data point for sample No.5 that occurs in both groups is the most rightone in both plot (a) and plot (b).

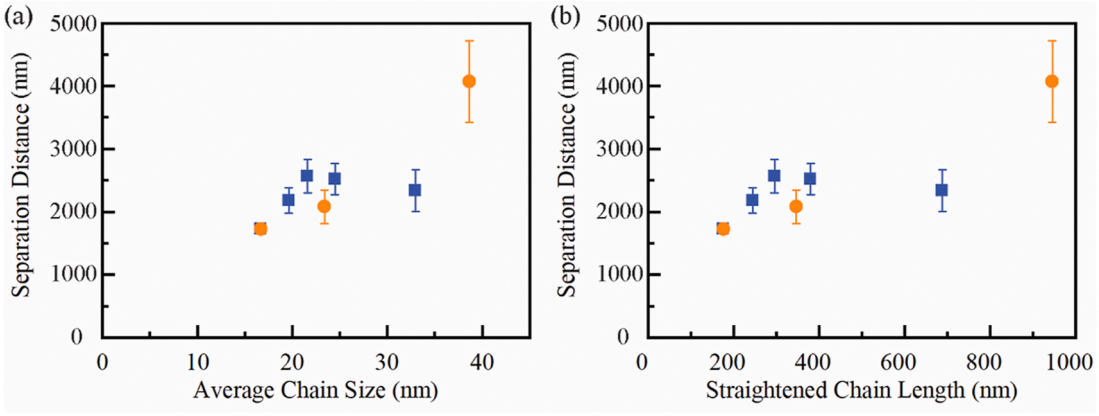

Fig. 10. (a) Separation distance versus the average chain size. (b) Separation distance versus the straightened chain length. Results are from the holding time of 180 s. The data point for sample No.5 that occurs in both groups is the most left one in both plot (a) and plot (b).

Declaration of competing interest

The authors declare that they have no known competing financial interests or personal relationships that could have appeared to influence the work reported in this paper.

Acknowledgment:

This work was supported by the National Science Foundation under Grant No. 2019783. Y. H. acknowledges funding support from the Air Force Office of Scientific Research under award number FA9550-19-1-0395.

Appendix A. Supplementary data

Supplementary data to this article can be found online at https://doi.org/10.1016/j.mechmat.2021.103877.

References

Bohdanecký, M., Petrus, V., Sedláček, B., 1983. Estimation of the characteristic ratio of polyacrylamide in water and in a mixed theta-solvent. Makromol. Chem. 184, 2061–2073. https://doi.org/10.1002/macp.1983.021841011.

Chakrabarti, A., Chaudhury, M.K., 2013. Direct measurement of the surface tension of a soft elastic hydrogel: exploration of elastocapillary instability in adhesion. Langmuir 29, 6926–6935. https://doi.org/10.1021/la401115j.

Flory, P.J., 1953. Principles of Polymer Chemistry. Cornell University Press.

Gennes, P.G. de, 1979. Scaling Concepts in Polymer Physics. Cornell University Press, NY.

Gong, J., Osada, Y., 1998. Gel friction: a model based on surface repulsion and adsorption. J. Chem. Phys. 109, 8062–8068. https://doi.org/10.1063/1.477453.

Gundogan, N., Okay, O., Oppermann, W., 2004. Swelling, elasticity and spatial inhomogeneity of poly(N,N- dimethylacrylamide) hydrogels formed at various polymer concentrations. Macromol. Chem. Phys. 205, 814–823. https://doi.org/10.1002/macp.200300174.

Hamzehlou, S., Reyes, Y., Leiza, J.R., 2013. A new insight into the formation of polymer networks: a kinetic Monte Carlo simulation of the cross-linking polymerization of S/DVB. Macromolecules 46, 9064–9073. https://doi.org/10.1021/ma4016054.

Han, S., Opdahl, A., Marmo, C., Somorjai, G.A., 2002. AFM and SFG studies of pHEMA-based hydrogel contact lens surfaces in saline solution: adhesion, friction, and the presence of non-crosslinked polymer chains at the surface. Biomaterials 23, 1657–1666.

He, D., Hu, Y., 2020. Nonlinear visco-poroelasticity of gels with different rheological parts. J. Appl. Mech. 87, 071010.

Hu, Y., Suo, Z., 2012. Viscoelasticity and poroelasticity in elastomeric gels. Acta Mech. Solida Sin. 25, 441–458. https://doi.org/10.1016/S0894-9166(12)60039-1.

Hu, Y., You, J.O., Auguste, D.T., Suo, Z., Vlassak, J.J., 2012. Indentation: a simple, nondestructive method for characterizing the mechanical and transport properties of pH-sensitive hydrogels. J. Mater. Res. 27, 152–160. https://doi.org/10.1557/jmr.2011.368.

Hu, Y., Zhao, X., Vlassak, J.J., Suo, Z., 2010. Using indentation to characterize the poroelasticity of gels. Appl. Phys. Lett. 96 https://doi.org/10.1063/1.3370354, 2009–2011.

Israelachvili, J.N., 2015. Intermolecular and Surface Forces. Academic press.

Johnson, K.L., Kendall, K., Roberts, A.D., 1971. Surface energy and the contact of elastic solids. Proc. R. Soc. Lond. A. Math. Phys. Sci. 324, 301–313.

Kalcioglu, Z.I., Mahmoodian, R., Hu, Y., Suo, Z., Van Vliet, K.J., 2012. From macro- to microscale poroelastic characterization of polymeric hydrogels via indentation. Soft Matter 8, 3393–3398. https://doi.org/10.1039/c2sm06825g.

Kii, A., Xu, J., Gong, J.P., Osada, Y., Zhang, X., 2001. Heterogeneous polymerization of hydrogels on hydrophobic substrate. J. Phys. Chem. B 105, 4565–4571. https://doi.org/10.1021/jp003242u.

Lai, Y., He, D., Hu, Y., 2019. Indentation adhesion of hydrogels over a wide range of length and time scales. Extrem. Mech. Lett. 31, 100540. https://doi.org/10.1016/j.eml.2019.100540.

Lai, Y., Hu, Y., 2018. Probing the swelling-dependent mechanical and transport properties of polyacrylamide hydrogels through AFM-based dynamic nanoindentation. Soft Matter 14, 2619–2627. https://doi.org/10.1039/c7sm02351k.

Lai, Y., Hu, Y., 2017. Unified solution for poroelastic oscillation indentation on gels for spherical, conical and cylindrical indenters. Soft Matter 13, 852–861. https://doi.org/10.1039/c6sm02341j.

Li, H., Choi, Y.S., Rutland, M.W., Atkin, R., 2020. Nanotribology of hydrogels with similar stiffness but different polymer and crosslinker concentrations. J. Colloid Interface Sci. 563, 347–353. https://doi.org/10.1016/j.jcis.2019.12.045.

Li, J., Hu, Y., Vlassak, J.J., Suo, Z., 2012. Experimental determination of equations of state for ideal elastomeric gels. Soft Matter 8, 8121–8128. https://doi.org/10.1039/c2sm25437a.

Lin, J., Lin, Y., Qian, J., 2014. Statistical pull off of nanoparticles adhering to compliant substrates. Langmuir 30, 6089–6094. https://doi.org/10.1021/la404153t.

Liu, Q., Suo, Z., 2016. Osmocapillary phase separation. Extrem. Mech. Lett. 7, 27–33. https://doi.org/10.1016/j.eml.2016.02.001.

Lu, J., Zhang, H., Yang, Y., 1993. Monte Carlo simulation of kinetics and chain-length distribution in radical polymerization. Macromol. Theory Simul. 2, 747–760. https://doi.org/10.1002/mats.1993.040020511.

Maugis, D., 1992. Adhesion of Spheres : the JKR-DMT transition using a dugdale model. J. Colloid Interface Sci. 150.

Pitenis, A.A., Urueña, J.M., Schulze, K.D., Nixon, R.M., Dunn, A.C., Krick, B.A., Sawyer, W.G., Angelini, T.E., 2014. Polymer fluctuation lubrication in hydrogel gemini interfaces. Soft Matter 10, 8955–8962. https://doi.org/10.1039/c4sm01728e.

Rubinstein, M., Colby, R.H., 2003. Polymer Physics. Oxford university press, New York.

Shoaib, T., Espinosa-Marzal, R.M., 2018. Insight into the viscous and adhesive contributions to hydrogel friction. Tribol. Lett. 66, 1–14. https://doi.org/10.1007/s11249-018-1045-7.

Wei, Y., 2014. A stochastic description on the traction-separation law of an interface with non-covalent bonding. J. Mech. Phys. Solid. 70, 227–241. https://doi.org/10.1016/j.jmps.2014.05.014.

Yang, Q.H., Qian, C.J., Li, H., Luo, M.B., 2014. Dynamics of a polymer adsorbed to an attractive homogeneous flat surface. Phys. Chem. Chem. Phys. 16, 23292–23300. https://doi.org/10.1039/c4cp03105a.